Two-dimensional snowflake trap for indirect excitons

Y. Y. Kuznetsova,[1] P. Andreakou,[1,2] M. W. Hasling,[1,*] J. R. Leonard,[1] E. V. Calman,[1] L. V. Butov,[1] M. Hanson,[3] and A. C. Gossard[3]

[1]Department of Physics, University of California at San Diego, La Jolla, California 92093-0319, USA

[2]Laboratoire Charles Coulomb, Université Montpellier 2, CNRS, UMR 5221, F-34095 Montpellier, France

[3]Materials Department, University of California at Santa Barbara, Santa Barbara, California 93106-5050, USA

*Corresponding author: mhasling@ucsd.edu

Received November 24, 2014; revised January 9, 2015; accepted January 9, 2015; posted January 13, 2015 (Doc. ID 226945); published February 10, 2015

We present experimental proof of principle for two-dimensional electrostatic traps for indirect excitons. A confining trap potential for indirect excitons is created by a snowflake-shaped electrode pattern. We demonstrate collection of indirect excitons from all directions to the trap center and control of the trap potential by voltage. © 2015 Optical Society of America

OCIS codes: (250.0250) Optoelectronics; (250.5590) Quantum-well, -wire and -dot devices.

http://dx.doi.org/10.1364/OL.40.000589

Potential traps made possible the realization of cold and dense atom gases and, eventually, the achievement of atom condensation. Traps also allow control of the confined gases by *in situ* varying the trap shape and depth. Similarly, potential traps are an effective tool for studying the physics of cold excitons–cold bosons in condensed matter materials.

The realization of a cold and dense exciton gas in a trap requires a long exciton lifetime, which allows excitons to travel to the trap center and cool to low temperatures before recombination. An indirect exciton in a coupled quantum well structure (CQW) is composed of an electron and a hole in spatially separated layers [Fig. 1(a)]. Lifetimes of indirect excitons are orders of magnitude longer than lifetimes of regular excitons, which allows the creation of trapping potentials where the indirect excitons are optically generated over the trap area and can reach the trap center. Although indirect excitons are typically hot when generated in the region of optical excitation, their long lifetimes allow them to cool below the temperature of quantum degeneracy a few nanoseconds after the generation [1] or a few micrometers away from the excitation spot [2]. Due to the small exciton mass, the temperature of quantum degeneracy for indirect excitons in GaAs CQW can be achieved at ∼1 K, which has allowed the observation of exciton condensation and spontaneous coherence in a trap at helium refrigerator temperatures [3].

Creating electrostatic traps for excitons requires control by voltage. Indirect excitons have a built-in dipole moment ed, where d is the separation between the electron and hole layers. As a result, their energy can be controlled by voltage: an electric field F_z perpendicular to the QW plane results in the exciton energy shift $-edF_z$ [4]. This gives the opportunity to realize the desired potential landscape for indirect excitons $E(x,y) = -edF_z(x,y)$ and control it by voltage *in situ*, on a time scale shorter than the exciton lifetime. Indirect excitons were studied in various electrostatically created potential landscapes including ramps [5–7], lattices [8–11], traps [3,12–21], and circuit devices [22–24].

Of particular interest is a trap that can provide a confining potential with the exciton energy gradually reducing toward the trap center. Such a confining potential could collect excitons from a large area, creating a dense exciton gas at the trap center. This, in turn, can facilitate the creation of a degenerate exciton gas in the trap since the temperature of quantum degeneracy is roughly proportional to the particle density. Furthermore, such potentials direct and confine excitons and, as a result, concentrate the energy transported via excitons thus operating as excitonic antennas. Directing and concentrating the energy can be explored in excitonic devices, for instance in molecular and polymeric solar cells [25].

Creating a trap with a confining in-plane potential on a large area is challenging. In this paragraph, we briefly overview the earlier studied electrostatic traps for indirect excitons. (i) A trap can be created by a circular opening in an electrode [13] or by a circular electrode [14,21]. In these traps, the in-plane potential varies within a small length from the electrode edge $\sim D$, where D is the distance between the top and bottom electrode [16]. Since D is typically small (1 μm in our samples) these traps produce a confining in-plane potential on a small area. Large traps of this type have a box-like shape [16]. (ii) A confining potential can be realized by laterally modulated voltage. These traps are produced by electrodes at different voltages and the exciton energy reduces from electrode to electrode toward the trap center [12,13,15,17–20]. The achievement of a large area of confining potentials in these traps requires a large number of separately contacted electrodes. In-plane voltage gradients in these traps may produce in-plane electric currents heating the excitons. (iii) Confining potentials for indirect excitons can be realized by using a single electrode: in earlier studies, this was achieved in the diamond-shaped traps [16]. The diamond-shaped traps offered the largest area for confining potentials studied so far. However, the elongated shape of the diamond traps limits the area of exciton collection, and as a result, limits the number of excitons collected in the trap center. In the earlier studies of exciton condensation and spontaneous coherence in the diamond trap, a total exciton number in the trap was limited to 10^3 [3].

In this work, we present experimental proof of principle for a new electrostatic trap for indirect excitons—the snowflake trap. The advantages of snowflake traps include the ability to produce a two-dimensional confining

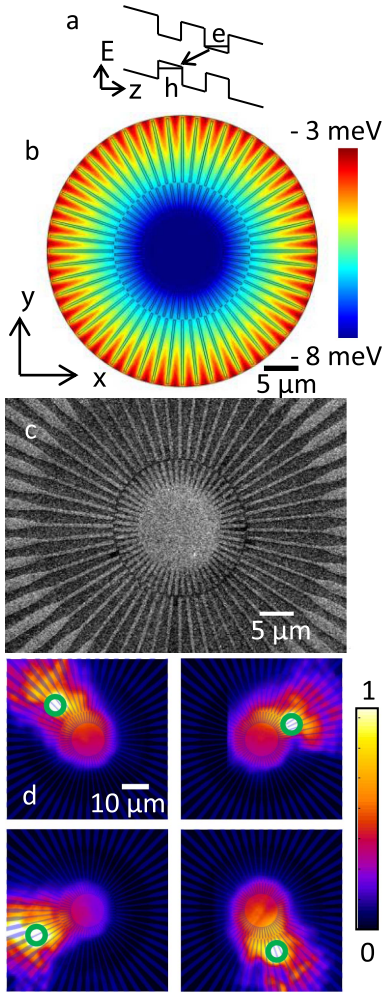

Fig. 1. (a) CQW diagram. e, electron; h, hole. (b) Calculated indirect exciton energy shift $E(x,y) = -edF_z(x,y)$ in the snowflake trap. Center and outer electrode voltage $V_c = V_o = -0.65$ V. (c) SEM image of the electrode pattern forming the snowflake trap for indirect excitons. (d) x–y emission images of indirect excitons for four different positions of the laser excitation spot. The excitation spot positions are given by green circles. The circle size corresponds to the excitation spot size. For each of the images in (d) the positions of the excitation spot and exciton emission cloud relative to the trap center are indicated by the overlayed electrode pattern (with the central part deleted for clarity). For all excitation spot positions, the generated excitons are effectively collected to the trap center by the trap potential. $V_c = -8$ V, $V_o = -6.5$ V, size of focused laser excitation spot $s = 7$ μm, excitation power $P \sim 50$ μW.

potential for indirect excitons on a large area, an order of magnitude larger than the diamond traps, using a single electrode with no exciton heating by in-plane electric currents. The operation principle of snowflake traps is based on the control of exciton energy by electrode density. The CQW is placed between a flat ground plane and a snowflake-shaped electrode, resulting in varying F_z in the CQW plane due to fringing electric fields from a shaped electrode. Decreasing electrode density toward the trap edges reduces F_z and, in turn, exciton energy shift, producing a confining potential for indirect excitons [26].

The structure was grown by molecular beam epitaxy. An n^+-GaAs layer with $n_{Si} = 10^{18}$ cm^{-3} served as a homogeneous bottom electrode. Mesas were etched to this layer in order to connect to it. The top electrodes were fabricated by depositing semitransparent 2 nm Ti - 7 nm Pt - 2 nm Au Au layers on the sample surface. These trap electrodes were covered by a layer of semitransparent insulation (300 μm thick SiO_2). Connecting electrodes (semitransparent 2 μm wide, 200 nm thick ITO) provided the contacts to the trap electrodes through 3×3 μm openings in the insulating layer. The electrode lines broaden out away from the center in the contact region for better contacts [Fig. 1(c)]. 700 nm wire-bondable Au pads with an ITO underlayer are connected to both the ITO electrodes and the etched area of the sample, creating connections to the trap electrodes and the ground plane. A pair of 8 nm GaAs QWs, separated by a 4 nm $Al_{0.33}Ga_{0.67}As$ barrier, was positioned 0.1 μm above the n^+-GaAs layer within an undoped $D = 1$ μm thick $Al_{0.33}Ga_{0.67}As$ layer. Positioning the CQW closer to the homogeneous electrode suppresses the in-plane electric field [13], which otherwise can lead to exciton dissociation.

The experiments were done at 1.6 K. Excitons were photogenerated by 700 nm Ti:sapphire laser. The emission images were taken by a nitrogen-cooled CCD camera. An interference filter selecting the spectral range of the indirect exciton emission was used for measuring x–y images. A spectrometer with resolution 0.18 meV was used for measuring x-energy images. The spatial resolution was 1.5 μm.

A snowflake trap can be created using a single snowflake-shaped electrode. However, in this work, the snowflake trap is formed by a snowflake-shaped pattern for a center electrode and separate outer electrodes. This allows us to control the shape of the confining potential by varying the voltages on the center and outer electrodes independently. The outer electrode pattern starts 10 μm from the trap center. An SEM image of the snowflake electrode pattern is presented in Fig. 1(c). The electrode density is adjusted to create a 2D in-plane potential profile for indirect excitons with the exciton energy gradually reducing toward the trap center from any direction.

Figure 1(b) shows the simulated exciton energy in the snowflake trap for a uniform voltage applied to the center and outer electrodes ($V_c = V_o = -0.65$ V). The simulations were done using COMSOL Inc. Multiphysics software. The simulations show a confining potential in all directions with an energy minimum at the trap center.

The emission of indirect excitons for four different positions of the laser excitation spot is presented in Fig. 1(d). The excitation spot positions are given by green circles. Figure 1(d) demonstrates the experimental proof of principle for the snowflake trap: for any position of the laser excitation spot, the generated excitons are effectively collected to the trap center by the trap potential.

Note that some excitons are also trapped toward the outside direction of the trap [Fig. 1(d)]. In this "contact region" outside the snowflake trap the electrodes become thicker for better contacts, which increases the electrode density and, as a result, lowers the exciton energy causing the "outside trapping."

We also studied the effect of varying voltage and excitation power on the trap profile. Figures 2(a)–2(c), 2(g)–2(i), and 3(a) and 3(c) demonstrate control of the

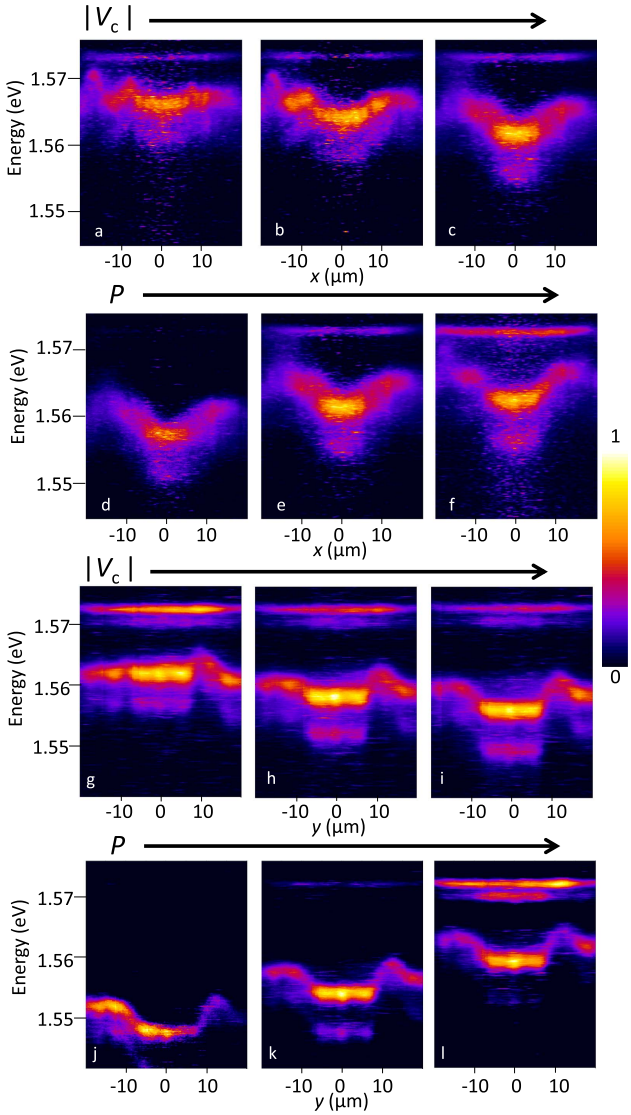

Fig. 2. (a)–(c) x-energy emission images versus center electrode voltage V_c. $V_c = -5$ (a), –6.5 (b), and –8 (c) V. Outer electrode voltage $V_o = -6.5$ V, excitation power $P \sim 100$ μW. (g)–(i) Similar data for the orthogonal direction. (d)–(f) x-energy emission images of indirect excitons versus P. $P \sim 20$ (d), 100 (e), and 500 (f) μW. $V_c = -8$ V, $V_o = -6.5$ V. (j)–(l) Similar data for the orthogonal direction. For all data, a defocused laser excitation with the spot size $s = 40$ μm is centered at the trap center. The emission at ~1.57 eV corresponds to spatially direct transitions. The emission of indirect excitons is observed at lower energies and is controlled by the trap potential and excitation power.

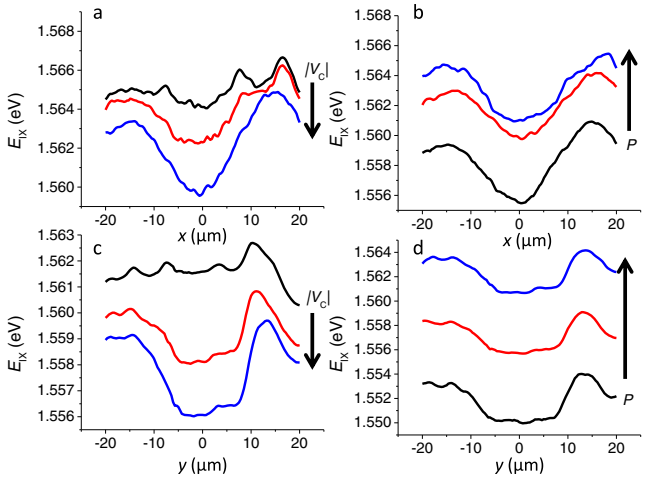

Fig. 3. (a) Profiles of average energy of indirect excitons in the snowflake trap for different center electrode voltages V_c. $V_c = -5$, –6.5, and –8 V. Outer electrodes are at $V_o = -6.5$ V, excitation power $P \sim 100$ μW. (b) Profiles of average energy of indirect excitons in the snowflake trap for different excitation powers P. $P \sim 20$, 100, and 500 μW. $V_c = -8$ V, $V_o = -6.5$ V. (c), (d) Similar data for the orthogonal direction. For all data, a defocused laser excitation with the spot size $s = 40$ μm is centered at the trap center.

shape of the snowflake trap by voltage. The reduction of absolute value of voltage on the center electrode V_c for fixed voltage on the outer electrode pattern V_o makes the trap shallower [Figs. 2(a), 2(g), and 2(a) and 2(c)]. Alternatively, increasing $|V_c|$, and keeping $|V_o|$ fixed makes the trap deeper and facilitates exciton collection to the trap center [Figs. 2(c) and 2(i), and Figs. 3(a) and 3(c)].

Figures 2(d)–2(f), 2(j)–2(l), and 3(b) and 3(d) show that as the density of indirect excitons increases, so does the exciton energy in the trap, and the trap becomes shallower. Such energy variation is consistent with the screening of the trap potential by the repulsively interacting indirect excitons. The repulsive interaction of indirect excitons originates from their built-in dipole moment [27]. Note, however, that even at the highest studied excitation powers the excitons do not screen the trap profile completely [Figs. 2(d)–2(f), 2(j)–2(l), and 3(b) and 3(d)].

The emission at ~1.57 eV corresponds to spatially direct transitions (Fig. 2). The spectra are measured in the defocused laser excitation spot. As discussed in the introduction [1,2], typically, excitons are hot in the laser excitation spot and, as a result, direct exciton emission is present in the spectrum.

The presented data demonstrate experimental proof of principle for snowflake traps. We note that the realized snowflake traps are not perfect: there is a disorder associated with the electrode imperfections originating from the electrode shape imperfections, surface charges, etc. The disorder is responsible for the deviation of the trap cross section from the simulated profile and for the difference in the trap cross sections in different directions. For instance, the trap cross sections in the two orthogonal directions have different shapes (Fig. 2). However, the disorder is not strong enough to compromise the major performance of the trap, namely, the ability to collect indirect excitons from all directions to the trap center [Fig. 1(d)]. The emission appearing below the main indirect exciton line (Fig. 2) can be related to localized states in a disorder potential of the structure. Lower energy emission lines in the studied CQW structure typically correspond to localized states [15].

The quality of electrode shape and the performance of the snowflake trap can be improved by increasing the lateral dimensions of the electrode pattern. For the same shape of the x–y confining potential, the lateral dimensions can be increased by proportionally increasing the distances between the CQW and top and bottom

electrodes [26]. Besides improving the trap quality, this can further increase the area of the confining potential: for instance, increasing D from 1 μm in the studied structure to 10 μm in future structures should increase the area of confining trap potential by 2 orders of magnitude. For a more efficient accumulation of indirect excitons to the center of such large traps, the lifetime of indirect excitons can be further enhanced by increasing the separation d between the QW layers. The development of snowflake traps forms the subject for future work.

In conclusion, we demonstrated experimental proof of principle for two-dimensional snowflake traps for indirect excitons which allow collecting a large number of excitons to the trap center. The operating principle of the snowflake trap is based on the lateral modulation of electrode density. We demonstrated collection of indirect excitons from all directions to the trap center and control of the trap shape by voltage.

We thank A. T. Hammack, M. Remeika, and M. Vladimirova for discussions, as well as Cal(it)^2 Nano3 staff for help with sample fabrication. This work was supported by NSF grant 0907349. P. A. was supported by EU ITN INDEX. Y. Y. K. was supported by an Intel Ph.D. Fellowship.

References

1. L. V. Butov, A. L. Ivanov, A. Imamoglu, P. B. Littlewood, A. A. Shashkin, V. T. Dolgopolov, K. L. Campman, and A. C. Gossard, Phys. Rev. Lett. **86**, 5608 (2001).
2. A. T. Hammack, M. Griswold, L. V. Butov, L. E. Smallwood, A. L. Ivanov, and A. C. Gossard, Phys. Rev. Lett. **96**, 227402 (2006).
3. A. A. High, J. R. Leonard, M. Remeika, L. V. Butov, M. Hanson, and A. C. Gossard, Nano Lett. **12**, 2605 (2012).
4. D. A. B. Miller, D. S. Chemla, T. C. Damen, A. C. Gossard, W. Wiegmann, T. H. Wood, and C. A. Burrus, Phys. Rev. B **32**, 1043 (1985).
5. M. Hagn, A. Zrenner, G. Böhm, and G. Weimann, Appl. Phys. Lett. **67**, 232 (1995).
6. A. Gärtner, A. W. Holleitner, J. P. Kotthaus, and D. Schuh, Appl. Phys. Lett. **89**, 052108 (2006).
7. J. R. Leonard, M. Remeika, M. K. Chu, Y. Y. Kuznetsova, A. A. High, L. V. Butov, J. Wilkes, M. Hanson, and A. C. Gossard, Appl. Phys. Lett. **100**, 231106 (2012).
8. S. Zimmermann, G. Schedelbeck, A. O. Govorov, A. Wixforth, J. P. Kotthaus, M. Bichler, W. Wegscheider, and G. Abstreiter, Appl. Phys. Lett. **73**, 154 (1998).
9. J. Krauß, J. P. Kotthaus, A. Wixforth, M. Hanson, D. C. Driscoll, A. C. Gossard, D. Schuh, and M. Bichler, Appl. Phys. Lett. **85**, 5830 (2004).
10. M. Remeika, J. C. Graves, A. T. Hammack, A. D. Meyertholen, M. M. Fogler, L. V. Butov, M. Hanson, and A. C. Gossard, Phys. Rev. Lett. **102**, 186803 (2009).
11. M. Remeika, M. M. Fogler, L. V. Butov, M. Hanson, and A. C. Gossard, Appl. Phys. Lett. **100**, 061103 (2012).
12. T. Huber, A. Zrenner, W. Wegscheider, and M. Bichler, Phys. Status Solidi A **166**, R5 (1998).
13. A. T. Hammack, N. A. Gippius, L. V. Sen Yang, G. O. Andreev Butov, M. Hanson, and A. C. Gossard, J. Appl. Phys. **99**, 066104 (2006).
14. G. Chen, R. Rapaport, L. N. Pffeifer, K. West, P. M. Platzman, S. Simon, Z. Vörös, and D. Snoke, Phys. Rev. B **74**, 045309 (2006).
15. A. A. High, A. T. Hammack, L. V. Butov, L. Mouchliadis, A. L. Ivanov, M. Hanson, and A. C. Gossard, Nano Lett. **9**, 2094 (2009).
16. A. A. High, A. K. Thomas, G. Grosso, M. Remeika, A. T. Hammack, A. D. Meyertholen, M. M. Fogler, L. V. Butov, M. Hanson, and A. C. Gossard, Phys. Rev. Lett. **103**, 087403 (2009).
17. G. J. Schinner, E. Schubert, M. P. Stallhofer, J. P. Kotthaus, D. Schuh, A. K. Rai, D. Reuter, A. D. Wieck, and A. O. Govorov, Phys. Rev. B **83**, 165308 (2011).
18. K. Kowalik-Seidl, X. P. Vögele, B. N. Rimpfl, G. J. Schinner, D. Schuh, W. Wegscheider, A. W. Holleitner, and J. P. Kotthaus, Nano Lett. **12**, 326 (2012).
19. G. J. Schinner, J. Repp, E. Schubert, A. K. Rai, D. Reuter, A. D. Wieck, A. O. Govorov, A. W. Holleitner, and J. P. Kotthaus, Phys. Rev. Lett. **110**, 127403 (2013).
20. G. J. Schinner, J. Repp, E. Schubert, A. K. Rai, D. Reuter, A. D. Wieck, A. O. Govorov, A. W. Holleitner, and J. P. Kotthaus, Phys. Rev. B **87**, 205302 (2013).
21. Y. Shilo, K. Cohen, B. Laikhtman, K. West, L. Pfeiffer, and R. Rapaport, Nat. Commun. **4**, 2335 (2013).
22. A. A. High, E. E. Novitskaya, L. V. Butov, M. Hanson, and A. C. Gossard, Science **321**, 229 (2008).
23. G. Grosso, J. Graves, A. T. Hammack, A. A. High, L. V. Butov, M. Hanson, and A. C. Gossard, Nat. Photonics **3**, 577 (2009).
24. P. Andreakou, S. V. Poltavtsev, J. R. Leonard, E. V. Calman, M. Remeika, Y. Y. Kuznetsova, L. V. Butov, J. Wilkes, M. Hanson, and A. C. Gossard, Appl. Phys. Lett. **104**, 091101 (2014).
25. G. M. Akselrod, P. B. Deotare, N. J. Thompson, J. Lee, W. A. Tisdale, M. A. Baldo, V. M. Menon, and V. Bulović, Nat. Commun. **5**, 3646 (2014).
26. Y. Y. Kuznetsova, A. A. High, and L. V. Butov, Appl. Phys. Lett. **97**, 201106 (2010).
27. C. Schindler and R. Zimmermann, Phys. Rev. B **78**, 045313 (2008).